Analysis of Large Nonregular Printed Scatterers Using the Contour-FFT

Simon Hubert, *Member, IEEE*, Shambhu Nath Jha, *Member, IEEE*, and Christophe Craeye, *Senior Member, IEEE*

***Abstract*— In fast Fourier transform (FFT)-based iterative methods for electromagnetic analysis of planar structures, the convolution between Green's function (GF) and the basis functions is carried out by a product in the spectral domain. In layered media, the GF is known analytically but exhibits singularities in the spectral domain, giving rise to numerical inaccuracy when processed by a direct FFT. We propose a direct spectral approach where the convolution is carried out with due account for the presence of a singular kernel. Using Contour-FFT, the integration contour is deformed and the spatial convolution is expressed as a rapidly converging series of FFTs. We also introduce a novel inverse Contour-FFT operator required for the process. As other FFT-based methods, the short-range interactions are corrected using a precomputed sparse operator, to which we propose an implementation compatible with the Contour-FFT. We control the accuracy of the method with a simple scheme that adapts the method's parameters to the problem at hand. Several practical numerical examples demonstrate the efficiency and accuracy of the method for the analysis of large nonregular printed structures.**

***Index Terms*— Antenna arrays, fast method, Fourier transforms, metasurfaces, method of moments (MoM), numerical analysis, reflectarrays.**

I. Introduction

FOR several decades, the method of moments (MoM) has been the method of choice for analyzing electromagnetic radiation and scattering by planar printed structures, despite its well-known limitations both in memory consumption and solving times. A lot of research has been carried out to reduce the computational effort of the classical MoM, resulting in a collection of fast methods. Many of these fast methods have been designed for the analysis of arrays of antennas or scatterers that consist of identical or similar elements [1]–[4], with impressive results in terms of time saving. However, when the structure considered does not present any particular symmetry, one cannot fully reap the benefits of these methods.

Manuscript received October 2, 2017; revised July 17, 2018; accepted July 30, 2018. Date of publication August 8, 2018; date of current version October 29, 2018. *(Corresponding author: Simon Hubert.)*

S. Hubert and C. Craeye are with the ICTEAM Institute, Université catholique de Louvain, 1348 Louvain-La-Neuve, Belgium (e-mail: smnhubert@gmail.com).

S. N. Jha was with ICOMS Detections SA, 1348 Ottignies-Louvain-la-Neuve, Belgium, and also with Université catholique de Louvain, 1348 Louvain-La-Neuve, Belgium. He is now with Thales Belgium, 1480 Tubize, Belgium.

Color versions of one or more of the figures in this paper are available online at http://ieeexplore.ieee.org.

Digital Object Identifier 10.1109/TAP.2018.2864314

To tackle the memory issue, one can rely on matrix-free Krylov subspace iterative methods [5]–[7]. These methods iteratively construct a solution subspace through successive matrix-vector products. The product of the interaction matrix with an arbitrary vector can be viewed as the convolution between the current distribution defined by the vector and Green's function (GF) associated with the medium, followed by testing of the resulting fields on a set of testing functions. The resulting vectors can thus be estimated without the need to compute the whole MoM interaction matrix. This provides a serious advantage in terms of time and memory complexity, as long as the number of iterations needed to reach the desired accuracy remains much smaller than the number of unknowns.

Several works initiated by [8]–[10] propose to use the fast Fourier transform (FFT) to perform the convolution between the GF and the current distribution through a product in the spectral domain, thus reducing the matrix-vector product time complexity from $\mathcal{O}(N^2)$ to $\mathcal{O}(N \log_2 N)$. An important milestone in the development of FFT-based methods was the adaptive integral method (AIM) [8], which introduced a precorrection technique (see below) to preserve high accuracy for very close interactions. $\mathcal{O}(N \log_2 N)$ complexities are also approached with kernel-independent techniques [11], although, generally, the knowledge of the applicable GF allows more compact field representations and better error control. Another widespread class of methods uses a multipole expansion of the currents to approximate the far fields: the multilevel fast multipole algorithm [12] also exhibits an $\mathcal{O}(N \log_2 N)$ complexity. Some optimized techniques even approach a linear complexity for specific dense problems [13]. However, the multilevel aspect of these methods requires complex implementations, whereas FFT-based convolution is more straightforward.

In the aforementioned FFT-based methods, it is clear that computing the convolution in the spectral domain provides a significant time saving for large systems of equations, as detailed in [8]-[10] and [14]-[18]. However, in those references, few comments have been raised concerning the accuracy of that discrete convolution, which requires special attention, given the wide spectrum of the GF and its slowly converging oscillatory nature. The latter can be associated with the singularities that appear in the Fourier transform of the GF [19]. Besides, when the spatial-domain GF is used, the numerical calculation of a Sommerfeld integral or the application of the discrete complex image method [20] can

also entail numerical errors. Finally, in the FFT-based convolution, in order to avoid aliasing, the space domain is usually doubled through zero padding in both directions.

In this paper, we directly express the convolution in the spectral domain, using the closed-form expression of the spectral GF for layered media [21]. This approach provides two main advantages over classical FFT-based methods. First, it avoids the spatial GF calculation over a regular grid. While spatial GF computation in layered media has been intensely studied (see [21]–[24] and references therein), the proposed method simply bypasses this step. Then, in favorable circumstances, the proposed approach may allow an accurate calculation of convolution without doubling the space domain, effectively reducing the number of space and spectral-domain samples, and thus the computation time and memory.

Such a direct spectral-domain approach supposes a proper treatment of the spectral singularity. The Contour-FFT [3] is a recent method conceived to quickly compute Fourier transforms of singular functions. It essentially combines the FFT and integration path deformation to properly compute convolutions with singular kernels. Its efficiency has already been proven [3] for the analysis of large irregular arrays of identical planar scatterers, where the interactions between predefined macro basis functions [25] are very efficiently tabulated versus relative positions.

One drawback of the spectral domain convolution is a less accurate evaluation of short-range interactions, due to the finite size of the FFT, truncating higher spectral components. This issue, common to all FFT-based methods, has been addressed in [16] and [26], where it is treated properly in the "precorrection" step of the algorithm. Essentially, the same approach is found in [1] where a sparse correction matrix is precomputed and used to compensate for the error at each iteration. This precorrection is capable of exactly compensating for the short-range errors, no matter their origin. The same principle is used in this paper, though we introduce a new formulation adapted to convolutions based on the Contour-FFT.

This paper proposes an iterative scheme using a novel Contour-FFT acceleration. The matrix-vector products are computed as follows: first, we expand the current distribution on a regular grid of points and evaluate its Fourier transform in the complex plane using an inverse Contour-FFT, and then, we evaluate the convolution with the GF using the Contour-FFT, which includes due treatment of spectral-domain singularities. The resulting field on the grid is tested on each testing function in the spatial domain, and finally, the short-range interactions are corrected using a precomputed sparse operator. A simple scheme to control the error is also demonstrated to adapt the method's parameters to a specific problem beforehand, and to determine the size of the short-range zone where the correction is applied. The resulting method is quite accurate and scales well with the number of unknowns, for arbitrary structures where no symmetry can be found.

The remainder of this paper is organized as follows. Section II provides details on every step of the proposed method. Section III summarizes the parameters governing the method's accuracy, and proposes a scheme to adapt them to a specific problem. Section IV presents validating examples as well as a comparison with other established FFT-based methods. Section V focuses on complexity analysis in larger problems, and Section VI concludes this paper.

II. Development of the Iterative Method

For the sake of completeness, all the steps of the method are described below. Some of them are already well established, whereas those exploiting the Contour-FFT are new. We consider a planar metallization printed on one interface of a layered medium, for simplicity. After expanding the metallization into N basis functions, such as rooftop or Rao–Wilton–Glisson (RWG) [27] basis functions, we express the MoM system of equations as

$$\mathbf{Zx} = -\mathbf{b} \tag{1}$$

with $\mathbf{Z} \in \mathbb{C}^{N\times N}$ the interaction matrix, and $\mathbf{x}$ and $\mathbf{b} \in \mathbb{C}^N$ the current distribution and excitation vectors, respectively. Each element of the interaction matrix $\mathbf{Z}$ is expressed as [28]

$$Z_{ij} = \iint_{S_i} \mathbf{f}_i(\mathbf{r}) \iint_{S_j} \mathbf{G}(\mathbf{r}-\mathbf{r}')\,\mathbf{f}_j(\mathbf{r}')\,d\mathbf{r}'\,d\mathbf{r} \tag{2}$$

with $\mathbf{f}_i$ the ith basis and testing functions (assuming a Galerkin testing procedure), $\mathbf{G}$ the dyadic space-domain GF, $\mathbf{r}$ and $\mathbf{r}'$ the observation and source vectors, respectively, and S_i the domain of the basis function i. Equivalently, the mixed-potential expression can be used [21]

$$\begin{aligned} Z_{ij} = \iint_{S_i}\iint_{S_j} & G_A(\mathbf{r}-\mathbf{r}')(\mathbf{f}_i(\mathbf{r})\cdot\mathbf{f}_j(\mathbf{r}')) \\ & + G_V(\mathbf{r}-\mathbf{r}')(\nabla\cdot\mathbf{f}_i(\mathbf{r}))(\nabla\cdot\mathbf{f}_j(\mathbf{r}'))\,d\mathbf{r}'\,d\mathbf{r} \end{aligned} \tag{3}$$

where it is emphasized that, for layered media, the scalar GFs G_A and G_V are different.

When a direct solution of (1) is not computationally feasible, an iterative scheme can approximate the solution with controllable accuracy. The well-known Krylov subspace-based iterative techniques [7] are based on the construction of a reduced matrix $\mathbf{Q}_n$ as

$$\mathbf{Q}_n = [\mathbf{b} \quad \mathbf{Zb} \quad \mathbf{Z}^2\mathbf{b} \quad \ldots \quad \mathbf{Z}^{n-1}\mathbf{b}]. \tag{4}$$

The reduced matrix (4) spanning the Krylov subspace can thus be computed iteratively, each iteration requiring only one matrix-vector product. At each iteration step, the vector obtained at the previous step is used as a current distribution and the new vector is obtained by testing the field generated by these currents on the testing functions. This operation is sped up in the proposed formulation, in the following way:

1) Expansion: The current distribution is expanded on a regular Cartesian grid of points [16]. This step is detailed in Section II-A.
2) Convolution: The 2-D Fourier transform of the whole current distribution is computed, and its spatial convolution with the GF is computed in the spectral domain. Section II-B details the formulation and highlights the accuracy problems that arise if the convolution is implemented as a simple FFT, due to the singular kernel.

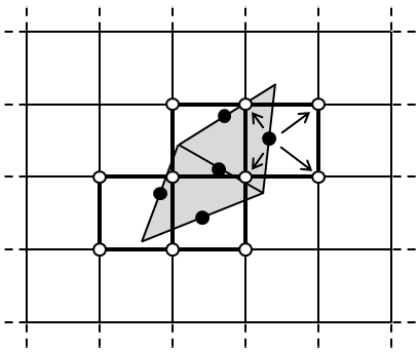

Fig. 1. Illustration of a first-order expansion scheme for a single RWG basis function. Lines: section of the regular grid. Plain dots: quadrature points (here, a 5-point middle-edge quadrature). Empty dots: grid points where the basis function is expanded. Arrows: 2×2 subgrid ($L = 2$) where the quadrature point is expanded.

Section II-C presents our contribution to solve these problems using the Contour-FFT.

3) Testing: The resulting radiated field is interpolated and integrated on each testing function. This step is the reciprocal of the Expansion step and is also detailed in Section II-A.
4) Correction: The short-range interactions are corrected using a precomputed sparse operator. To this end, the precorrection step described in [16] is adapted for the specific formulation developed in the three previous steps. This new correction algorithm is detailed in Section II-D.

A. Distribution and Testing Scheme

As in [8] and [16], we define a Cartesian grid of $M \times M$ points equally spaced at distances Δx, Δy from each other in each direction of space, which covers the entire domain of metallization. Each basis function is then projected on that Cartesian grid using Lagrange polynomials of arbitrary orders. To ease its implementation, this procedure is presented here in more detail, and illustrated in Fig. 1.

1) To each basis function, $\mathbf{f}_j(\mathbf{r}')$ is assigned a set of quadrature points (x_g, y_g) and weights w_g. The number of points can vary for larger or smaller basis functions. For RWG and rooftop basis functions, Gauss or Dunavant quadratures [29] can be used for instance.
2) For each quadrature point, we select the square subgrid of L^2 points (x_l, y_l) centered around the quadrature point.
3) Each point of this subgrid is assigned a vectorial weight $\hat{\mathbf{f}}$ such that

$$[\hat{\mathbf{f}}_j]_g = \mathbf{f}_j(x_g, y_g) S_j \, l_l(x_g) l_l(y_g) w_g \tag{5}$$

with $l_l(x)$ the Lagrange polynomial associated with the lth subgrid point and S_j the surface of the jth basis function. The Lagrange interpolation is then of order $L - 1$.
4) If a subgrid point is used by more than one quadrature point, the weights are simply summed up, resulting in the expansion of each basis function into a tiny set of weights $\hat{\mathbf{f}}_j$ on the grid as

$$\hat{\mathbf{f}}_j = \sum_g [\hat{\mathbf{f}}_j]_g. \tag{6}$$

These weights are precomputed and will be used for both the Expansion and Testing steps. Assuming again a Galerkin procedure, the source and testing functions form a unique set of basis functions, and thus the weights are the same. This procedure is similar to [1] with one important difference: here, we use Lagrange polynomials to expand the basis functions on the grid and to interpolate the field for the testing phase, but not to approximate the spatial GF for long-range interactions, since we never explicitly construct the spatial GF. In addition, we observed that using the same set of weights and points for the Expansion and Testing steps produced more accurate results than nonsymmetrical operators.

Note that the time needed for the expansion and testing steps scales linearly with the number of unknowns; the time and memory complexity of these steps is thus $\mathcal{O}(N)$.

B. Spectral Acceleration

The convolution, which corresponds to the inner integral of (2), can be expressed in the Fourier domain as

$$Z_{ij} = \iint_{S_i} \mathbf{f}_i(\mathbf{r}) \, \mathcal{F}^{-1}\{\widetilde{\mathbf{G}}(k_x, k_y) \, \widetilde{\mathbf{f}}_j(k_x, k_y)\} d\mathbf{r} \tag{7}$$

with $\widetilde{\mathbf{G}}$ and $\widetilde{\mathbf{f}}_j$ denoting the Fourier transform of the dyadic GF $\mathbf{G}$ and the basis function, respectively. Note that the spectral GF $\widetilde{\mathbf{G}}$ is known analytically for any layered substrate [21].

Entry i of the resulting matrix-vector product in (4) is then expressed as

$$[\mathbf{Zb}]_i = \iint_{S_i} \mathbf{f}_i \cdot \mathcal{F}^{-1} \left\{ \widetilde{\mathbf{G}} \, \mathcal{F} \left\{ \sum_{j=1}^{N} b_j \mathbf{f}_j \right\} \right\} d\mathbf{r} \tag{8}$$

which, assuming a $e^{j\omega t}$ time dependence, is realized as

$$[\mathbf{Zb}]_i \approx \iint \hat{\mathbf{f}}_i \cdot \mathrm{FFT} \left\{ \widetilde{\mathbf{G}} \, \mathrm{FFT}^{-1} \left\{ \sum_{j=1}^{N} b_j \hat{\mathbf{f}}_j \right\} \right\} d\mathbf{r}. \tag{9}$$

In that way, the Fourier transform of the complete current distribution is obtained with a single FFT. Note that, in this paper, all FFTs are 2-D. The computation complexity of that operation and the convolution with the GF thus reduces to $\mathcal{O}(M^2 \log_2 M^2)$.

The spectral GF $\widetilde{\mathbf{G}}$ in (9) may cause numerical inaccuracy if $\mathcal{F}^{-1}$ is implemented using a simple FFT and the sampling points are close to its poles. Section II-C presents our contribution to solving this problem.

C. Direct and Inverse Contour-FFT

We will first recall the principles of the Contour-FFT for the case of an inverse Fourier transform of the singular integrand $\widetilde{H}$, that is

$$H(x, y) = \frac{1}{4\pi^2} \iint \widetilde{H}(k_x, k_y) \, e^{-j(k_x x + k_y y)} \, dk_x \, dk_y. \tag{10}$$

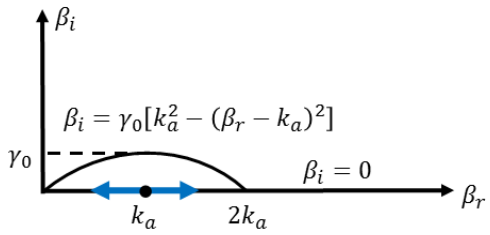

Fig. 2. Quadratic contour used for the integration path. The imaginary part of the radial spectral variable β_i is expressed as a function of its real part β_r. $k_a = k_0\sqrt{\epsilon_a} = 2\pi/\lambda_a$ is the average wavenumber with $\epsilon_a = (\epsilon_r + 1)/2$.

The $\widetilde{H}$ function varies rapidly near its poles, which greatly complicates its numerical integration. One possibility to smoothen the integrand of (10) is to use a contour deformation to push the integration path away from the poles. Assuming that all the poles lie inside a centered circle of radius $2k_a$ in the (k_x, k_y) plane, the contour of Fig. 2 can be used along the radial spectral direction. As proven in [3], (10) still can be expressed in terms of the real Cartesian coordinates (k_x, k_y) as

$$H(x,y) = \frac{1}{4\pi^2}\iint \widetilde{H}(k_x^c, k_y^c)\, e^{-j(k_x x + k_y y)} e^{(k_x^i x + k_y^i y)} C(k_x, k_y)\, dk_x\, dk_y \quad (11)$$

where k_x, k_y and k_x^i, k_y^i are, respectively, the real and imaginary parts of the complex wavenumbers k_x^c, k_y^c, and

$$C(k_x, k_y) = \left(1 + j\frac{d\beta_i}{d\beta_r}\right)\left(1 + j\frac{\beta_i}{\beta_r}\right) \quad (12)$$

where $\beta_r = ({k_x}^2 + {k_y}^2)^{1/2}$ is the radial wavenumber and β_i is its imaginary part defined by the contour in Fig. 2.

Expression (11), despite properly treating the poles, cannot be evaluated using the FFT because of the real exponential factor that contains spectral and spatial variables that are not separable. To overcome this drawback, that factor is expanded into a Taylor series of the spatial variables (x, y) around $(0, 0)$, resulting in a rapidly converging series of FFTs as

$$H(x,y) \approx K' \sum_{t=0}^{T} \frac{1}{t!} \sum_{t'=0}^{t} P_t^{t'} x^{t'} y^{t-t'} \mathrm{FFT}\{\gamma^t k_x^{t'} k_y^{t-t'} \widetilde{H}'\} \triangleq \mathrm{CFFT}_T\{\widetilde{H}\} \quad (13)$$

where T is the order of the Taylor expansion, $P_t^{t'}$ is Pascal's triangle element, $\gamma = \beta_i/\beta_r = k_x^i/k_x = k_y^i/k_y$ is defined as the local height of the contour, and

$$\widetilde{H}'(k_x^c, k_y^c) = (-1)^{k_1+k_2}\, C(k_x, k_y)\, \widetilde{H}(k_x^c, k_y^c) \quad (14)$$

$$K' = (-1)^{k_1+k_2} \frac{\Delta k_x \Delta k_y}{4\pi^2}. \quad (15)$$

The factors Δk_x, Δk_y and k_1, k_2 are, respectively, the spacing and index of the point in the spectral grid and result from the change of variables (see [3, Appendix A] for a rigorous definition).

Note that both the spectral GF and the Fourier transform of the currents need to be evaluated at the complex wavenumbers (k_x^c, k_y^c) according to the integration contour. This is not an issue for the GF, which is known in closed form. However, some special attention has to be paid to the Fourier transform of the currents. To this end and to preserve the speed-up advantages of the FFT, the principles of the Contour-FFT can be applied to the inverse transform. This leads to an inverse Contour-FFT operator, derived here for the first time. Following the same development as in (10)–(15), we start by expressing the Fourier transform $\widetilde{H}$ evaluated in the complex spectral variables (k_x^c, k_y^c), that is:

$$\widetilde{H}(k_x^c, k_y^c) = \iint H(x,y)\, e^{j(k_x x + k_y y)}\, e^{-(k_x^i x + k_y^i y)}\, dx\, dy \quad (16)$$

where the real and imaginary parts of k_x^c and k_y^c have already been separated. Once again, this expression cannot be evaluated directly using the FFT because of the real exponential factor, containing spectral and spatial variables. Expanding that factor into a Taylor series, we obtain a rapidly converging series of inverse FFTs. This brings us to the inverse Contour-FFT transformation, defined as

$$\widetilde{H}(k_x^c, k_y^c) \approx \mathrm{CFFT}_T^{-1}\{H\} \triangleq K'' \sum_{t=0}^{T} \frac{(-\gamma)^t}{t!} \sum_{t'=0}^{t} P_t^{t'} k_x^{t'} k_y^{t-t'} \mathrm{FFT}^{-1}\{x^{t'} y^{t-t'} H'\} \quad (17)$$

with

$$H'(x,y) = (-1)^{n_1+n_2}\, H(x,y) \quad (18)$$

$$K'' = (-1)^{n_1+n_2} M^2\, \Delta x \Delta y. \quad (19)$$

Again, the factors n_1, n_2 are the indices of the point in the spatial grid and result from the change of variables.

The complete expression for the approximation of the matrix-vector products in (4) using the Contour-FFT is then

$$[\mathbf{Zb}]_i \approx [\widehat{\mathbf{Zb}}]_i \approx \iint \hat{\mathbf{f}}_i \cdot \mathrm{CFFT}_T \left\{ \widetilde{\mathbf{G}}\, \mathrm{CFFT}_T^{-1} \left\{ \sum_{j=1}^{N} b_j \hat{\mathbf{f}}_j \right\} \right\} d\mathbf{r}. \quad (20)$$

The number of FFT evaluations in (13) and (17) for a Taylor-series order of T is $(T+1)(T+2)$; the time complexity for the expression (20) is thus $\mathcal{O}(T^2\ M^2 \log_2\ M^2)$.

For comparison, matrix-vector products evaluated with FFT-based methods, such as the AIM [8], can be expressed as

$$[\mathbf{Zb}]_i \approx \iint \hat{\mathbf{f}}_i \cdot \mathrm{FFT} \left\{ \mathrm{FFT}^{-1}\{\mathbf{G}\}\, \mathrm{FFT}^{-1} \left\{ \sum_{j=1}^{N} b_j \hat{\mathbf{f}}_j \right\} \right\} d\mathbf{r} \quad (21)$$

where the spectral GF, $\mathrm{FFT}^{-1}\{\mathbf{G}\}$ (instead of $\widetilde{\mathbf{G}}$), is obtained from samples precomputed in the space domain. To avoid aliasing in (21), the domain of the FFT must be twice as large as the computation domain, in both the directions.

A discussion about the effect of each parameter of the method on complexity and accuracy is presented in Section III. However, it is observed that the computation remains inaccurate. This is due to the crude truncation of the spectral

integration domain inherent to the FFT approach, which leads to inaccurate short-range interactions. Section II-D proposes a way to overcome this issue, building on precorrection techniques [8], [16].

D. Correction of Short-Range Interactions

As introduced in [8] and adapted to printed structures in [16], a sparse matrix $\mathbf{P}$ is precomputed to correct the inaccurate short-range interactions. In the context of the proposed method, this correction can be written as

$$P_{ij} = Z_{ij} - \iint \hat{\mathbf{f}}_i \cdot \mathrm{CFFT}_T\left\{\widetilde{\mathbf{G}}\ \mathrm{CFFT}_T^{-1}\{\hat{\mathbf{f}}_j\}\right\} d\mathbf{r} \tag{22}$$

for expanded testing functions $\hat{\mathbf{f}}_i$, which are "close" to the source functions $\hat{\mathbf{f}}_j$; this criterion will be discussed in Section III. The first term in the right-hand side of (22) is the exact MoM interaction matrix element defined in (2), and the second one is the matrix-vector product defined in (20) with only one pair of source and testing functions involved. Including this correction step, the final expression of the matrix-vector product is

$$\mathbf{Z}\,\mathbf{b} \approx \widehat{\mathbf{Z}\,\mathbf{b}} + \mathbf{P}\,\mathbf{b}. \tag{23}$$

For very large problems, the rightmost matrix-vector product in (23) is computationally feasible, since the correction matrix $\mathbf{P}$ is sparse, requiring the evaluation of only a tiny subset of elements of the MoM interaction matrix. The naive computation of the second term in the right-hand side of (22) would require carrying out a complete Contour-FFT operation for each basis function. That would defeat the purpose of the iterative solver, i.e., the amount of matrix-vector products has to remain much smaller than the number of unknowns. In the next paragraphs, we propose an alternative formulation that greatly reduces the time needed for that operation.

Since the elements of (22) only concern source and testing functions that are spatially close to each other, for each source point, only a very small subset of the spatial grid is used as test points. Reasoning in the spatial domain allows the exploitation of this observation by rearranging the order of operations. The result is an optimized algorithm for the evaluation of the sparse correction matrix without losing any accuracy. We start by expressing the spectral convolution by injecting (13) and (17) into the rightmost term of (22). Since the development of the CFFT and its inverse consists of linear combinations of FFTs, we use the linearity property of the FFT to move the sums and the constants in front of the expression. After rearranging, the discretized field in (22) becomes

$$\begin{aligned}&\mathrm{CFFT}\{\widetilde{\mathbf{G}}\ \mathrm{CFFT}^{-1}\{\hat{\mathbf{f}}_j\}\}\\ &\quad= \sum_t \frac{(-1)^t}{t!} \sum_{t'} P_t^{t'} \sum_u \frac{1}{u!} \sum_{u'} P_u^{u'} x^{u'} y^{u-u'}\, \mathbf{F}_j(u,u',t,t')\end{aligned} \tag{24}$$

with

$$\begin{aligned}&\mathbf{F}_j(u,u',t,t')\\ &\quad= \mathrm{FFT}\left\{\gamma^{\,u+t} k_x^{u'+t'} k_y^{u+t-u'-t'} \widetilde{\mathbf{G}}'\ \mathrm{FFT}^{-1}\left\{\hat{\mathbf{f}}_j\, x'^{t'} y'^{t-t'}\right\}\right\}\end{aligned} \tag{25}$$

with (x, y) and (x', y') denoting, respectively, the observation (testing) and source points. Using the circular convolution properties of the discrete Fourier transform [30], the latter Fourier transform can be reinterpreted as a discrete spatial convolution and is rewritten as

$$\begin{aligned}&\mathbf{F}_j(u,u',t,t')\\ &\quad= \sum_q \mathbf{G}_{u'+t'}^{u+t}(x-x_q, y-y_q)\ \hat{\mathbf{f}}_j(x_q,y_q)\ x_q^{t'}\, y_q^{t-t'}\end{aligned} \tag{26}$$

where q are the indices of the points on the grid expanding the basis function $\hat{\mathbf{f}}_j$, and $\mathbf{G}_b^a$ is a single term of the series (13), that is

$$\mathbf{G}_b^a(x,y) = \mathrm{FFT}\left\{\gamma^{\,a} k_x^b k_y^{a-b}\, \widetilde{\mathbf{G}}'\left(k_x^c, k_y^c\right)\right\}. \tag{27}$$

The final expression for the correction matrix is then

$$P_{ij} = Z_{ij} - \sum_p \hat{\mathbf{f}}_i(x_p,y_p) \cdot \sum_q \mathbf{G}_{p,q}^{mod}\ \hat{\mathbf{f}}_j(x_q,y_q) \tag{28}$$

where the modified spatial GF $\mathbf{G}_{p,q}^{mod}$ has to be computed for each pair of points (p, q) sufficiently "close" to each other, and is defined as

$$\begin{aligned}\mathbf{G}_{p,q}^{mod} &= \mathbf{G}^{mod}(x_p,y_p,x_q,y_q)\\ &= \sum_{t=0}^{T} \frac{(-1)^t}{t!} \sum_{t'=0}^{t} P_t^{t'} x_q^{t'} y_q^{t-t'}\\ &\quad\times \sum_{u=0}^{T} \frac{1}{u!} \sum_{u'=0}^{u} P_u^{u'} x_p^{u'} y_p^{u-u'} \mathbf{G}_{t'+u'}^{t+u}(x_p-x_q, y_p-y_q).\end{aligned} \tag{29}$$

The matrices defined by (27) are precomputed for the small subset of spatial distances (x, y) defined as the "short-range" zone and for every order $a, b \in [0, 2T]$.

Finally, symmetries are considered to further reduce the memory and time consumption in this optimization. Indeed, (29) is the reciprocal and exhibits a double-axial symmetry, which leads to the following equalities:

$$\mathbf{G}_{p,q}^{mod} = \mathbf{G}_{-p,q}^{mod} = \mathbf{G}_{p,-q}^{mod} = \mathbf{G}_{-p,-q}^{mod} = \mathbf{G}_{q,p}^{mod} \tag{30}$$

and means that (28) can be evaluated for up to eight pairs of points with a single evaluation of the quadruple sum (29).

Since (28) is just a reformulation of (22), the two expressions are rigorously equivalent. We indeed observed that short-range interactions are corrected within machine precision.

III. Error Control

The accuracy of the proposed method relies on an informed choice of a set of parameters summarized here.

1) M^2: The number of points in the square Cartesian grid.
2) k_{max}: The maximum spectral component in the grid. Together with M, these two parameters fully determine the characteristics of the spectral and spatial grids through the constraints that the FFT imposes on the sampling points in both the domains.
3) γ_0: The height of the quadratic contour defined in Fig. 2.
4) T: The order of the Taylor expansion for the Contour-FFT and its inverse.

5) L: The order of the Lagrange expansion of the basis functions.

An exhaustive analysis of the effect of the first four parameters on the evaluation of planar GFs can be found in [31] and [32], and a complete error model related to free-space planar GF has been developed in [33]. To summarize that work, the evaluation is more accurate in a certain range from the source when increasing γ_0, and that range increases with the order T. At very short range, the radius of the zone over which the correction is necessary is inversely proportional to k_{max}. It has also been observed that the envelope of the relative error is constant on the whole chosen spatial domain when the ratio

$$k_{max}/M\,\gamma_0 \tag{31}$$

is kept constant.

To control the error and estimate the radius of the "short-range" zone for a given problem, we rely on the comparison between the spatial GF estimated by the Contour-FFT and a reference solution. The latter is computed using a classical numerical integration scheme such as a Hankel transform with contour deformation and a safe amount of integration points to ensure accuracy [31]. Since this reference solution is computed once and for all for a given substrate, the execution time is not critical and does not need to be optimized. By changing the aforementioned parameters following the guidelines in [31]–[33], one can manage to fit the targeted accuracy level over the desired domain. This is illustrated in Fig. 3. We observe that the accuracy mask is not respected in G_A for distances smaller than $0.55\lambda_a$: this defines the "short-range" zone where the correction operation will be applied.

It is interesting to note that the parametrization algorithm described in [32] assumes a sequential implementation. That is, if the series of FFTs in (13) can be carried out in parallel, then a higher contour and fewer integration points (smaller FFTs) may be chosen. Indeed, higher contours are less sensitive to integration difficulties such that a lower density of spectral points can be afforded.

This procedure is simple and efficient, and offers a worst case scenario estimation of the Contour-FFT accuracy on the domain of interest. Indeed, in the iterative scheme, the spectral GF is first multiplied by the Fourier transform of the current distribution before being processed, as expressed in (20). This product by a band-limited spectrum attenuates higher spectral components, and thus reduces the impact of the truncation of the spectral domain inherent to the FFT approach. This filtering by the current distribution is mentioned in [3] and has a positive impact on the accuracy of the Contour-FFT.

Note that this procedure does not consider the distribution and the testing scheme (see Section II-A), characterized by the Lagrange order L. However, numerical experiments showed that for most typical sets of parameters, the accuracy does not seem to improve much beyond $L = 2$.

IV. Validation

For validation purposes, two representation examples will be provided in this section, followed by a comparison with an approach based on the AIM.

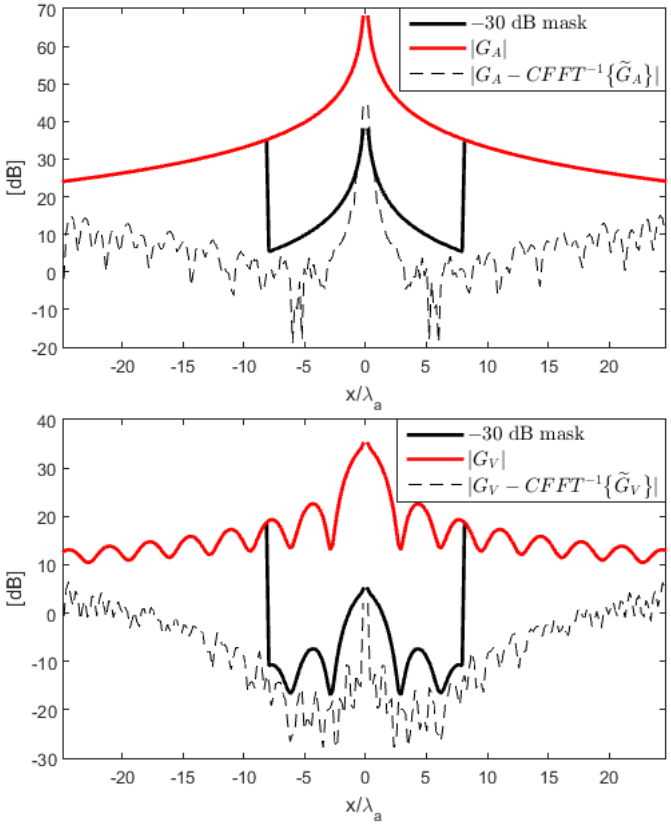

Fig. 3. Example of error estimation by comparison between the scalar spatial GF defined in (3) estimated with the Contour-FFT and a reference solution. The −30 dB mask is defined for $\rho < 8\lambda_a$. Single layer substrate with $\epsilon_r = 9.8$ and thickness $d = \lambda_0/12$, backed with PEC. Method parameters: $M = 256$, $k_{max} = 6\ k_0$, $\gamma_0 = k_0/340$, and $T = 2$.

A. Array of Random Patches

First, we analyze the port currents and embedded radiation patterns of a regular array of 169 patches of random sizes and orientations, pictured in Fig. 4. The patches are printed on a single-layer substrate with permittivity $\epsilon_r = 2.2$ and thickness $d = \lambda_0/20$, and they are fed by a delta-gap source in the middle of a stripline extension, as can be seen in Fig. 5. For this example, the "short-range" zone is defined as one array cell. That is, the correction step is carried out only on the self-interaction of each patch. The method parameters are selected according to the guidelines described in [31] and [32] and summarized in Section III to achieve −30 dB of accuracy on the whole domain of the array (excluding the short-range zone), and the following parameters are obtained: $M = 1024$, $k_{max} = 8k_0$, $\gamma_0 = k_0/600$, and $T = 2$. To accelerate the convergence of the iterative method, a block-diagonal preconditioner is implemented using the short-range interaction matrices Z_{ij} already computed in (22).

Figs. 6–8 present the embedded radiation patterns and currents at the ports, as a comparison between the iterative solver and the classical MoM solution used as a reference. For the sake of comparison, the difference between the MoM and three different methods is displayed:

1) the proposed Contour-FFT method;
2) the same iterative scheme with contour deformation and using a simple FFT (that is, $\gamma_0 \neq 0$ and $T = 0$);

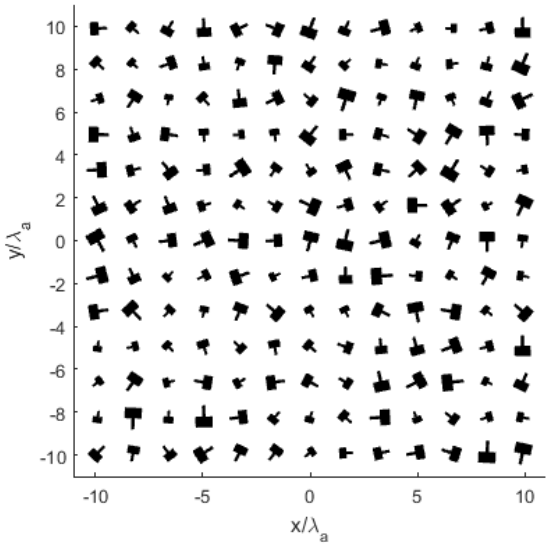

Fig. 4. Array of 13×13 scaled patches. The elements are $1.65\lambda_a$ apart in the x- and y-directions and the total number of unknowns is 22 101.

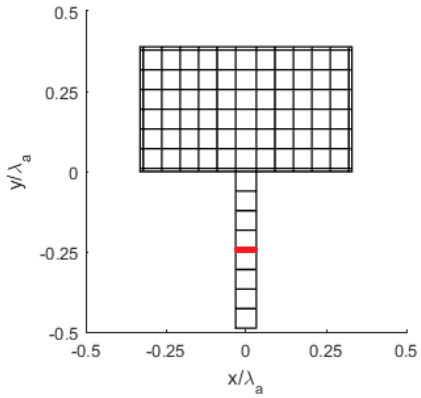

Fig. 5. Details of one patch element, meshed with rooftop basis functions. The delta-gap source is highlighted in red.

3) the same iterative scheme without contour deformation and using a simple FFT (that is, $\gamma_0 = 0$ and $T = 0$).

We observe that the error is much lower with the proposed Contour-FFT scheme, with the targeted accuracy of -30 dB respected on the majority of the port currents (exceptions mainly concern extremely low port current values). The embedded pattern is also very well estimated. Note that the solution produced by the third solver (simple FFT without contour deformation) is highly inaccurate for most of the port currents.

Table I summarizes the execution times' distribution for the three methods. We note that the computation of the sparse interaction matrix needed for the correction on the short-range zone and the preconditioner is still by far the bottleneck; however, it only requires the evaluation of 0.66% of the elements of the full MoM matrix.

Fig. 9 presents a comparison of the solvers' execution times and number of iterations, and Fig. 10 compares convergence rates. From these, we observe that the number of iterations is almost double for the simple FFT method. That is, the more accurately the matrix vectors are estimated, the faster the solution converges. This is an important result that justifies the small overhead due to the computation of a series of

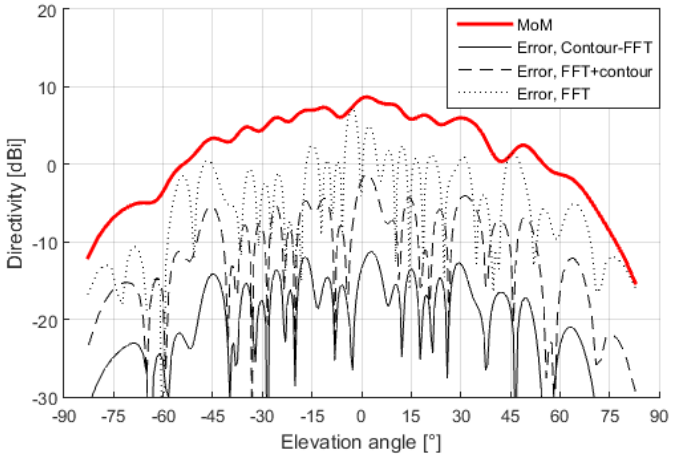

Fig. 6. Directivity of the embedded element pattern of the center element of the array, E-plane cut ($\phi = 0°$). Error is the absolute value of the difference between the directivities obtained with MoM solution and with the three solvers.

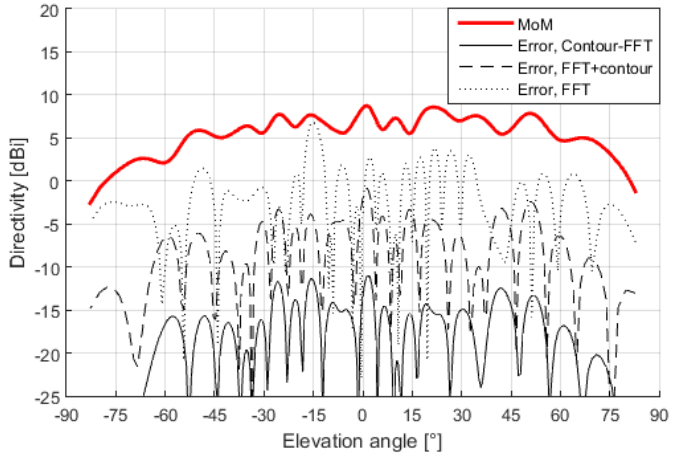

Fig. 7. Directivity of the embedded element pattern of the center element of the array, H-plane cut ($\phi = 90°$).

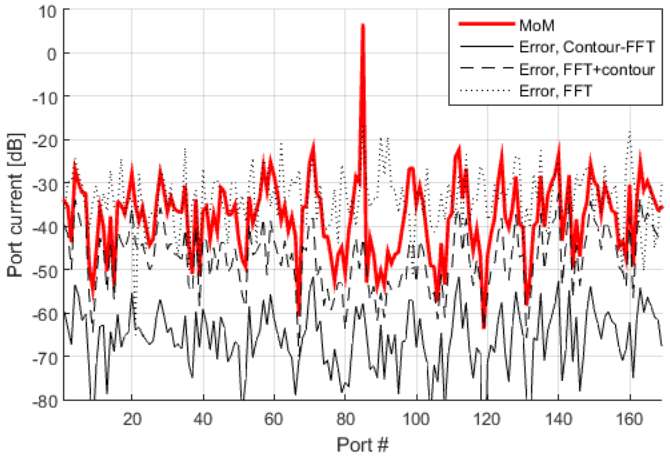

Fig. 8. Port currents (in dB) of each of the 13×13 patches, arranged rowwise.

TABLE I
COMPARISON OF EXECUTION TIMES IN SECONDS

	Common	Contour-FFT	FFT w/contour	FFT
Sparse matrix	1173			
Preconditioner	0.35			
Other	131			
Correction matrix		28.7	27.4	27.6
Iterative solver		83.9	62.4	119
Patterns	39.5			

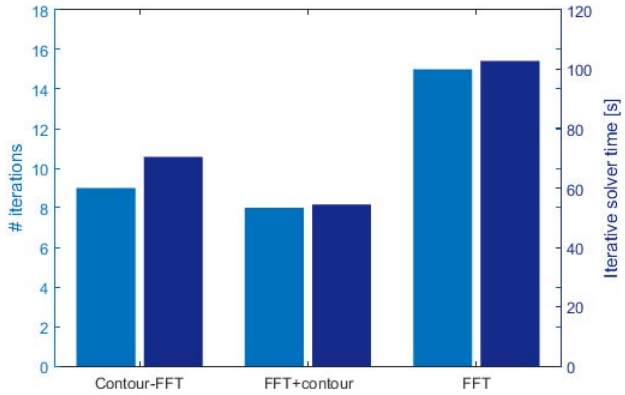

Fig. 9. Comparison of the three iterative solvers: amount of iterations and execution time. The solution has converged each time with a normalized residual criterion of −150 dB.

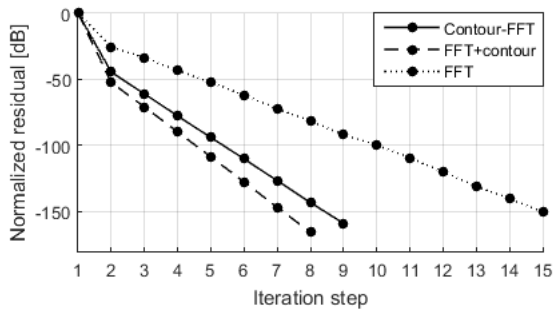

Fig. 10. Convergence rate for the three solvers. The solvers were stopped at a normalized residual of −150 dB.

FFTs at each iteration, which is inherent to the proposed method. In addition, the solver is a bit slower for the proposed scheme, compared with the second solver, but the solution error achieved by that second solver is far above the initially targeted −30 dB.

B. Scattering by a Large Ring

For the second example, we analyze the scattering by a large ring printed on a single-layer dielectric substrate with permittivity $\epsilon_r = 9.8$ and thickness $d = \lambda_0/12$, illuminated by a linearly polarized plane wave normally incident to the surface of the patch. The parameters used are the same as in Fig. 3, that is: $M = 256$, $k_{max} = 6\ k_0$, $\gamma_0 = k_0/340$, and $T = 2$. The metallization is meshed with RWG basis functions and displayed in Fig. 11.

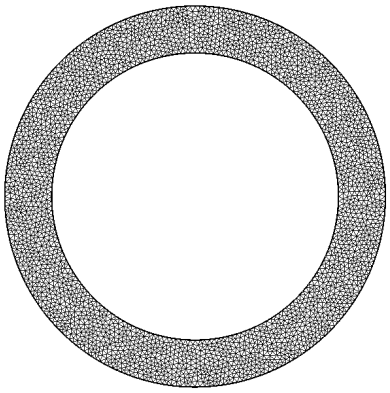

Fig. 11. Mesh of the second example: the inner and outer radii are $3\lambda_a$ and $4\lambda_a$, respectively. The total number of unknowns is 10 605.

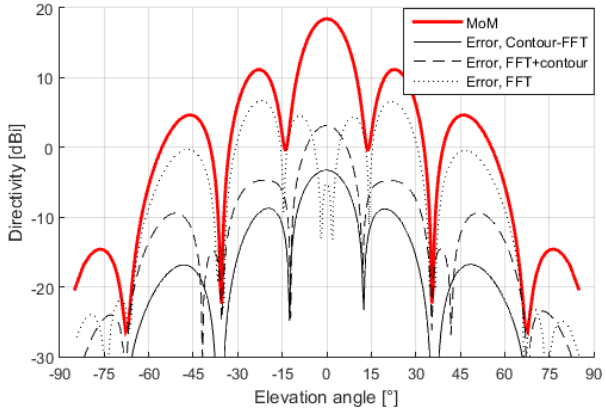

Fig. 12. Directivity of the electric field scattered by the ring, E-plane cut ($\phi = 0°$).

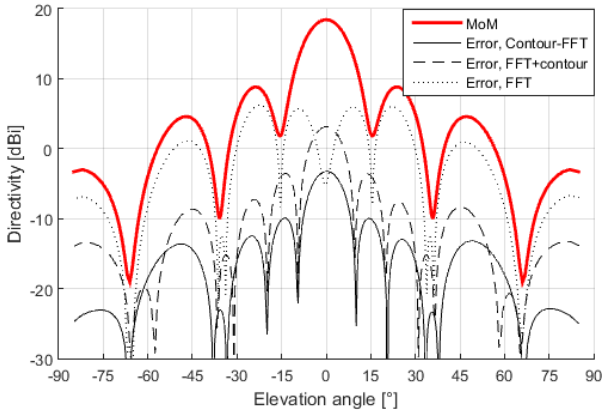

Fig. 13. Directivity of the electric field scattered by the ring, H-plane cut ($\phi = 90°$).

Since this is a fully connected structure, a special attention is paid to the definition of short-range interactions. We start by dividing the mesh into hexagonal subdomains. For each source subdomain, we define the six adjacent subdomains (and itself) as neighbors of the source subdomain. The correction matrix (22) is then computed for every pair of basis functions lying in neighboring subdomains. To ensure that every interactions outside the short-range zone is accurate,

the diameter of one hexagonal subdomain has to extend at least over the "short-range zone": in this case $0.45\lambda_a$. The same zone is used for the computation of a shielded block diagonal preconditioner [34], [35], again to reuse Z_{ij} required in (22).

As with the previous example, Figs. 12 and 13 present the scattered fields obtained with the three different solvers, compared with the reference solution obtained with the classical MoM. As above, the accuracy is much better with the proposed method. However, here, the solution converges in about 400 iterations in each case. This high and constant number indicates that the implemented shielded-block preconditioner is not very well suited to these connected structures. Nevertheless, the solver does converge, with a gain of more than 15 dB in relative accuracy on most secondary lobes compared with the simple FFT solver.

C. Comparison With AIM-Based Method

This section aims at relating the respective performance of the proposed method with previously developed FFT-based techniques. The proposed iterative method based on the matrix-vector product in (20) is thus compared with the AIM approach [8], [16], based on expression (21). Note that the latter approach corresponds to a circular (or cyclic) convolution [30]: the spatial domain needs to extend to twice the area of the actual current distribution in order to avoid aliasing effects. This phenomenon is well described in [15]. The specificity of the Contour-FFT is to bypass that spatial approach, for which aliasing is inherent. The proposed method should thus compute matrix-vector products efficiently, using smaller FFT grids. This observation adds up to the already mentioned advantages of the availability of an accurate error model, and of avoiding the computation of the spatial GF on all grid points.

In both the methods tested below, the projection and interpolation scheme based on Lagrange polynomials and presented in Section II-A is used to obtain $\hat{\mathbf{f}}_i$. This means that (21) does not exactly correspond to the formulation in [16], where the projection operator is based on matching the vector potential on a set of points around the basis function.

We first compared both approaches on the normal operating conditions of AIM, that is, with the spatial domain extending to twice the computation domain. The parametrization algorithm described in Section III and [32] sometimes creates this configuration for two connected reasons. First, based on (31), increasing k_{max} leads to a higher contour, and thus to a larger Taylor order (13) to maintain accuracy at long distances.[1] Second, in a sequential implementation, to avoid that larger Taylor order, doubling the number of spectral points can be computationally more efficient, but leads to a wider spatial domain. This situation typically occurs with thin substrates, for which large spectral components are needed to catch the sharp spatial singularity. In this case of a zero-padded spatial domain, we observed that both the methods produce very similar results in terms of accuracy and convergence.

[1]A low contour with a lower density of spectral points near the singularity(ies) may degrade the accuracy (see also Fig. 2).

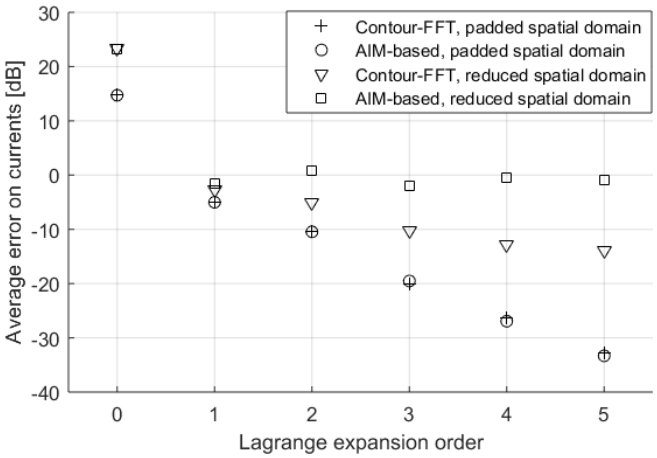

Fig. 14. Average relative error on the current distribution, after convergence, for both the proposed and AIM-based approaches.

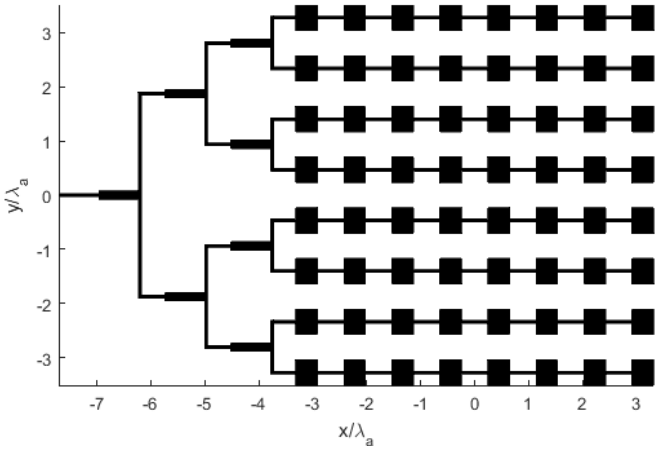

Fig. 15. Example of an 8×8 series-fed patch array. Dimensions from [36]. The structure is fed at the extreme left with a delta-gap source and a $\lambda/4$ microstrip extension. The frequency is 9.42 GHz.

TABLE II
SIMULATED SERIES-FED MICROSTRIP ARRAY CONFIGURATIONS

#	Array size	FFT size	T	Unknowns	Iterations
1	2×2	512×512	3	945	10
2	8×4	512×512	3	7531	69
3	8×8	512×512	4	14251	89
4	8×12	1024×1024	2	20971	103
5	16×8	1024×1024	2	28732	166
6	16×16	1024×1024	3	55612	214
7	32×16	2048×2048	2	111604	407

The advantages of the Contour-FFT method for the case of very thin substrates may thus be limited, at least if the parametrization algorithm is followed systematically.

However, for the case of thick substrates, the parametrization algorithm suggests spatial grids that fit more tightly the computation domain. We then also compared both the approaches using this reduced spatial domain. The chosen structure is similar to that in Section IV-A: we generated a regular array of 169 patch antennas presented in Fig. 5, with a randomized scale factor and an orientation angle. The array is $10.8\lambda_0$ wide, but now, the substrate has a permittivity of

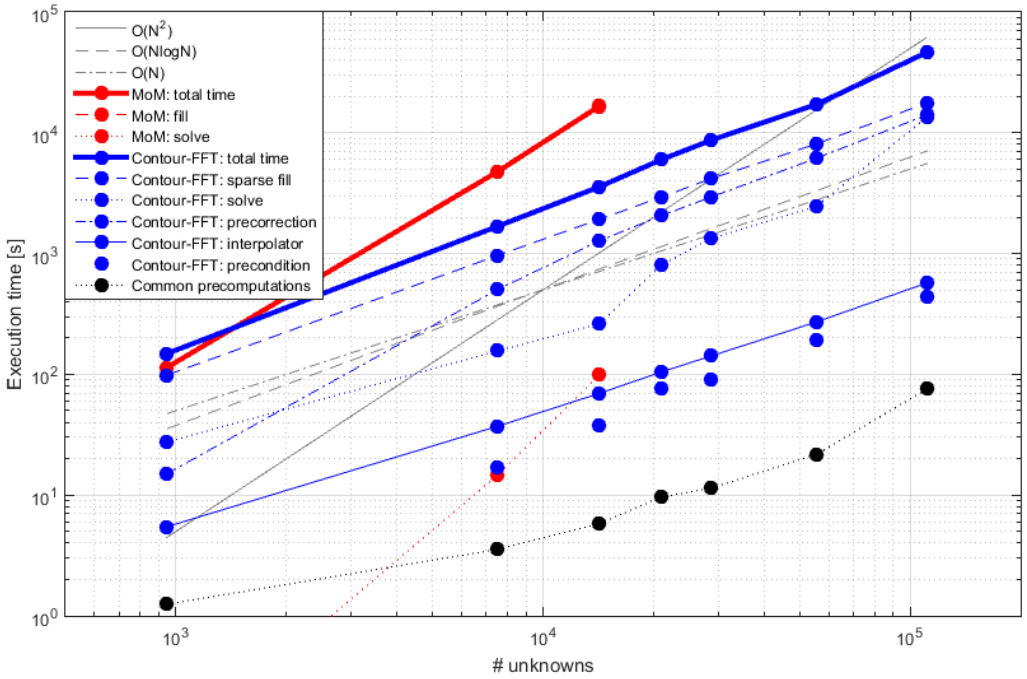

Fig. 16. Execution time distribution for the array of series-fed patches. Thick lines: total execution times for the proposed iterative method and for classical MoM (for smaller problems). Thin lines: each step of the method. For classical MoM, the matrix filling curve is hidden behind total time curve.

$\epsilon_r = 4$ and is $0.3\lambda_0$ thick. We analyzed the current distribution on this array fed at its central element, using both the proposed and AIM-based methods, compared with a classical MoM. As mentioned before, for each method, two situations are investigated: the "reduced spatial domain" that fits the computation domain as prescribed by the parametrization algorithm and the "padded spatial domain" that extends to twice the computation domain. The "reduced" set of parameters is $M = 128$, $k_{max} = 4\,k_0$, $\gamma_0 = k_0/150$, and $T = 4$.

The results are summarized in Fig. 14. Note that this configuration exhibits a rather coarse spatial grid, which is why the results strongly depend on the order of the Lagrange expansion (5). We observe that the AIM-based method is inaccurate with the reduced spatial domain because of aliasing, to which the Contour-FFT method is much less subjected. The two methods produce essentially the same results when the domain is padded with zeros.

V. Scaling

This section presents results for larger problems with a focus on the scaling of execution times with the number of unknowns. As the method is designed for arbitrary structures, for the sake of demonstration, there are no other specific optimizations implemented compared with those mentioned in Section II.

The first series of examples consists of arrays of series-fed patches inspired from [16] and [36]. Fig. 15 presents an example of a small 8×8 array, and Table II summarizes the configurations of the simulated arrays and the parameters obtained to reach a target accuracy of -30 dB. The substrate is 1.575 mm thick and has a permittivity of $\epsilon_r = 2.2$.

Due to the connections between patches, the interactions of each patch on itself and its eight neighbors are corrected and the corresponding shielded-block preconditioner is implemented (see Section IV-B). Finally, the convergence criterion is fixed at -150 dB (normalized residual).

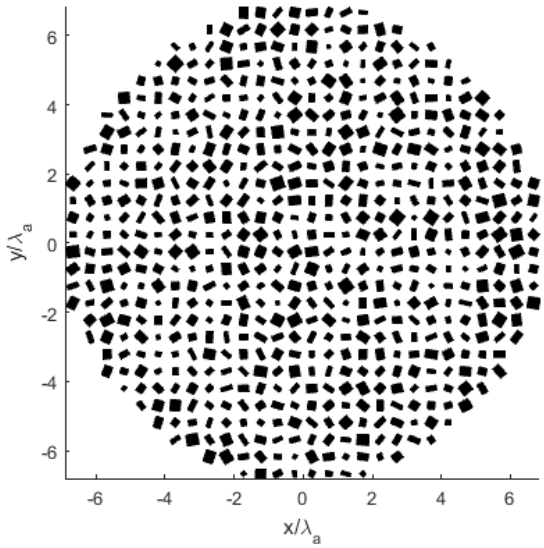

Fig. 17. Example of a 616 element array of random patches. The array is illuminated by a circularly polarized plane wave with 30° incidence.

TABLE III
Simulated Random Patches Array Configurations

#	Diameter	Elements	FFT size	T	Unknowns	Iterations
1	$5\lambda_a$	80	256×256	3	4001	12
2	$7\lambda_a$	156	512×512	2	7933	17
3	$10\lambda_a$	316	512×512	3	16983	27
4	$14\lambda_a$	616	512×512	4	32447	32
5	$20\lambda_a$	1264	1024×1024	3	65509	47
6	$30\lambda_a$	2828	2048×2048	3	147352	72

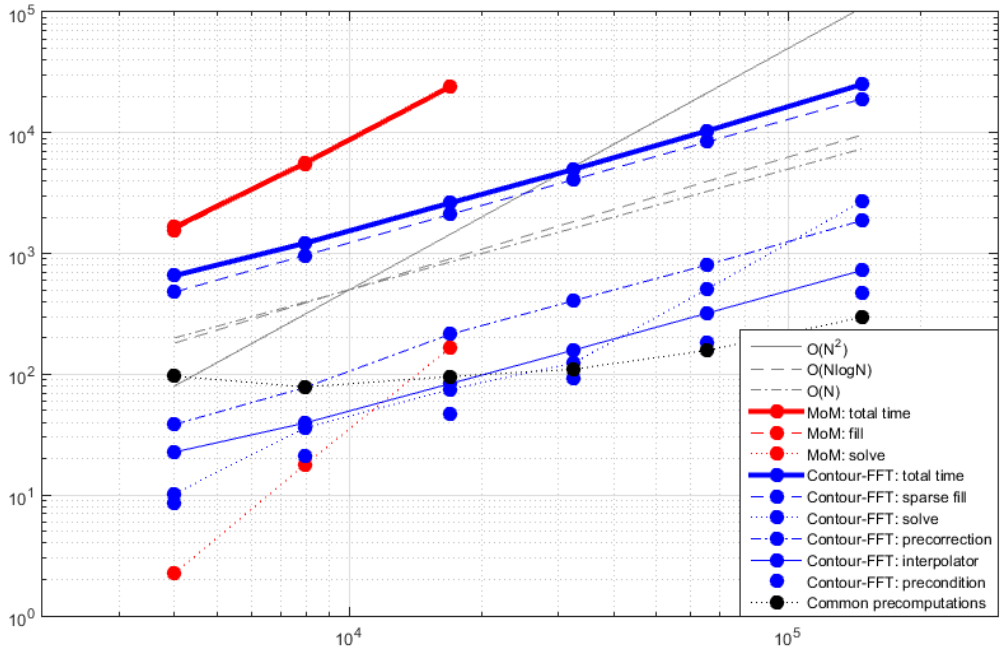

Fig. 18. Execution time distribution for the circular array of random patches. Thick lines: total execution times for the proposed iterative method and for classical MoM (for smaller problems). Thin lines: each step of the method. For classical MoM, the matrix filling curve is hidden behind total time curve.

Fig. 16 summarizes the solution times with the proposed Contour-FFT iterative method, and provides a comparison with the MoM for problems small enough to fit into 16 GB of memory. For those, the mean error on the current distribution compared with the MoM ranges from -40 to -34 dB for a target accuracy of -30 dB, which confirms the worst case scenario behavior of parametrization.

We observe from the execution times' distribution (Fig. 16) that the longest steps concern the computation of the correction matrix [that is, both the terms in the right-hand side of (22)], and that these durations grow mostly linearly with the number of unknowns. As a result, the total time exhibits also a mostly linear behavior. Regarding the solver time, the trend is piecewise linear, with a step at each increase in the FFT size. This results in a difficult to predict complexity.

In the second series of examples, we analyze scattering by a printed regular array of rectangular patches with random dimensions and rotation angles, such as the one presented in Fig. 17. The substrate is the same as in the previous example, and the whole structure is illuminated by a circularly polarized plane wave with a 30° incidence at 24 GHz. The same criteria for tuning, convergence, correction, and precondition are used as well.

The configurations analyzed are summarized in Table III and the execution times' distribution is plotted in Fig. 18. As with the previous example, the mean error on the current distribution varies between -37.5 and -32 dB. We note that this problem converges in substantially fewer iterations, probably because each patch is isolated, which results in a better conditioning of the initial system of equations. Also the correction matrix is computed much faster with this configuration, leaving the computation of short-range interactions as the sole dominant part of the execution time. The same comments about the trends of execution times can be made.

It should be noted that all the numerical results presented in this paper were computed on a typical desktop computer. Nevertheless, critical optimizations can be developed to further reduce the computation time. First, the implementation is written partly in MATLAB [37] and in C++ languages, both sharing information via a simple file-based protocol. This impacts primarily the distribution of the current on the spatial grid, which currently takes approximately 70% of the time at each iteration. The language of implementation also has an impact on the computation of the correction matrix, though to a lesser extent. Last, most of the code does not support multicore processors, which are now quite standard and could divide the overall execution time by a nonnegligible factor, especially for highly parallelizable operations such as the sparse matrix filling. Addressing these issues would considerably accelerate the aforementioned steps.

VI. Conclusion

FFT-based convolution is already in use for several decades for the fast MoM analysis of planar structures. In general, those methods first estimate the spatial GF from the analytical spectral GF, and then compute the convolution in the spectral domain via an FFT. The main contribution of this paper consists of a way to directly use the analytical spectral GF in the convolution, obliterating the need to compute the spatial GF on every spatial point. That is made possible with the help of the Contour-FFT, which allows the computation of FFTs of singular functions with controllable accuracy, using integration on a complex-plane path, which is not directly compatible with the FFT algorithm. The inverse Contour-FFT operator is also

introduced, enabling FFTs evaluated in complex spectral coordinates, again with controllable accuracy. We also proposed an algorithm for the computation of the sparse correction matrix dealing with short-range interactions, as well as an efficient scheme for finding the method parameters to reach a given target accuracy.

The proposed method is capable of high accuracy, with a mean error on the current distribution lower than -30 dB, when compared with the classical MoM. The radiated far fields are also very well estimated using the Contour-FFT method, with much better results than direct spectral methods using a simple FFT. The time complexity is almost linear with respect to the number of unknowns for very large problems. It is also shown that, provided that the system of equations is well-conditioned, the Contour-FFT method provides a better approximation of the matrix-vector products and increases the convergence rate of the iterative solver and the accuracy of the converged solution, than direct spectral methods using a simple FFT. Connected problems still exhibit a slower convergence rate, which could be tackled in a future communication through the implementation of a better suited preconditioner.

In terms of accuracy and convergence, the performance of the proposed direct method is similar to that of already established FFT-based methods in the observed thin-substrate cases. However, the advantages of the Contour-FFT method have been demonstrated for planar structures on thick substrates, for which the proposed method is able to compute matrix-vector products using smaller FFTs. In addition, in a parallel implementation with each Taylor term computed on a different core, higher contours requiring fewer spectral points can be afforded, leading to significantly smaller FFT sizes.

Finally, in the context of arbitrary structures, a large fraction of the computation time and memory resources may still consist of computing explicit interactions between basis functions in the near-field zone and the associated spectral correction. Those near-field operations may be reduced at the expense of a wider spatial spectrum (see Section III, and [32] and [33]), with observed maximum distances ranging from $\lambda_a/4$ to $\lambda_a/10$. Further research will be needed to approach the quasi-static limit. We also note that contrary to the iterative part of the solver, these operations can be straightforwardly parallelized.

The method presented in this paper is readily applicable to a wide range of planar layered structures, ranging from classical phased arrays to reflectarrays or metasurfaces, and is suitable for the fast analysis of printed structures with arbitrary metallization or arrays with different elements.

ACKNOWLEDGMENT

The authors would like to thank D. Tihon from the Université catholique de Louvain for his wise comments and suggestions during the redaction of this paper.

REFERENCES

[1] B. J. Fasenfest, F. Capolino, D. R. Wilton, D. R. Jackson, and N. J. Champagne, "A fast MoM solution for large arrays: Green's function interpolation with FFT," *IEEE Antennas Wireless Propag. Lett.*, vol. 3, no. 1, pp. 161–164, Dec. 2004.

[2] G. Minatti, S. Maci, P. De Vita, A. Freni, and M. Sabbadini, "A circularly-polarized isoflux antenna based on anisotropic metasurface," *IEEE Trans. Antennas Propag.*, vol. 60, no. 11, pp. 4998–5009, Nov. 2012.

[3] S. N. Jha and C. Craeye, "Contour-FFT based spectral domain MBF analysis of large printed antenna arrays," *IEEE Trans. Antennas Propag.*, vol. 62, no. 11, pp. 5752–5764, Nov. 2014.

[4] E. Erçil, L. Alatan, and Ö. A. Civi, "An efficient numerical solution method for reflectarrays of varying element sizes," *IEEE Trans. Antennas Propag.*, vol. 63, no. 12, pp. 5668–5676, Dec. 2015.

[5] W. C. Chew, J.-M. Jin, E. Michielssen, and J. Song, Eds., *Fast and Efficient Algorithms in Computational Electromagnetics*. Norwood, MA, USA: Artech House, 2001.

[6] C. Craeye and D. González-Ovejero, "A review on array mutual coupling analysis," *Radio Sci.*, vol. 46, no. 2, pp. 1–25, Apr. 2011.

[7] H. A. van der Vorst, "Krylov subspace iteration," *Comput. Sci. Eng.*, vol. 2, no. 1, pp. 32–37, Jan./Feb. 2000.

[8] E. Bleszynski, M. Bleszynski, and T. Jaroszewicz, "AIM: Adaptive integral method for solving large-scale electromagnetic scattering and radiation problems," *Radio Sci.*, vol. 31, no. 5, pp. 1225–1251, Sep. 1996.

[9] M. F. Catedra, J. G. Cuevas, and L. Nuño, "A scheme to analyze conducting plates of resonant size using the conjugate-gradient method and the fast Fourier transform," *IEEE Trans. Antennas Propag.*, vol. AP-36, no. 12, pp. 1744–1752, Dec. 1988.

[10] T. Sarkar, E. Arvas, and S. Rao, "Application of FFT and the conjugate gradient method for the solution of electromagnetic radiation from electrically large and small conducting bodies," *IEEE Trans. Antennas Propag.*, vol. AP-34, no. 5, pp. 635–640, May 1986.

[11] D. Gope and V. Jandhyala, "Efficient solution of EFIE via low-rank compression of multilevel predetermined interactions," *IEEE Trans. Antennas Propag.*, vol. 53, no. 10, pp. 3324–3333, Oct. 2005.

[12] R. Coifman, V. Rokhlin, and S. Wandzura, "The fast multipole method for the wave equation: A pedestrian prescription," *IEEE Antennas Propag. Mag.*, vol. 35, no. 3, pp. 7–12, Jun. 1993.

[13] D. Vande Ginste, H. Rogier, F. Olyslager, and D. De Zutter, "A fast multipole method for layered media based on the application of perfectly matched layers—The 2-D case," *IEEE Trans. Antennas Propag.*, vol. 52, no. 10, pp. 2631–2640, Oct. 2004.

[14] K. Yang and A. E. Yılmaz, "A three-dimensional adaptive integral method for scattering from structures embedded in layered media," *IEEE Trans. Geosci. Remote Sens.*, vol. 50, no. 4, pp. 1130–1139, Apr. 2012.

[15] B. J. Fasenfest, F. Capolino, and D. R. Wilton, "A fast MoM solver (GIFFT) for large arrays of microstrip and cavity-backed antennas," in *Proc. IEEE AP-S Int. Symp.*, Washington, DC, USA, Jul. 2005, pp. 6–9.

[16] N. Yuan, T. S. Yeo, X.-C. Nie, and L. W. Li, "A fast analysis of scattering and radiation of large microstrip antenna arrays," *IEEE Trans. Antennas Propag.*, vol. 51, no. 9, pp. 2218–2226, Sep. 2003.

[17] J. R. Phillips and J. K. White, "A precorrected-FFT method for electrostatic analysis of complicated 3-D structures," *IEEE Trans. Comput.-Aided Des. Integr. Circuits Syst.*, vol. 16, no. 10, pp. 1059–1072, Oct. 1997.

[18] V. Okhmatovski, M. Yuan, I. Jeffrey, and R. Phelps, "A three-dimensional precorrected FFT algorithm for fast method of moments solutions of the mixed-potential integral equation in layered media," *IEEE Trans. Microw. Theory Techn.*, vol. 57, no. 12, pp. 3505–3517, Dec. 2009.

[19] M. F. Catedra and E. Gago, "Spectral domain analysis of conducting patches of arbitrary geometry in multilayer media using the CG-FFT method," *IEEE Trans. Antennas Propag.*, vol. 38, no. 10, pp. 1530–1536, Oct. 1990.

[20] F. Ling and J.-M. Jin, "Discrete complex image method for Green's functions of general multilayer media," *IEEE Microw. Guided Wave Lett.*, vol. 10, no. 10, pp. 400–402, Oct. 2000.

[21] K. A. Michalski and J. R. Mosig, "Multilayered media Green's functions in integral equation formulations," *IEEE Trans. Antennas Propag.*, vol. 45, no. 3, pp. 508–519, Mar. 1997.

[22] M. I. Aksun, A. Alparslan, and K. A. Michalski, "Current status of closed-form Green's functions in layered media composed of natural and artificial materials," in *Proc. Int. Conf. Electromagn. Adv. Appl.*, Sep. 2009, pp. 451–454.

[23] H. Yang and A. E. Yılmaz, "Accuracy preserving computation of asymptotically smoothed layered medium Green's functions in finite precision arithmetic," in *Proc. IEEE Int. Symp. Antennas Propag. USNC/URSI Nat. Radio Sci. Meeting*, San Diego, CA, USA, Jul. 2017, pp. 1353–1354.

[24] K. Konno, Q. Chen, and R. J. Burkholder, "Fast computation of layered media Green's function via recursive Taylor expansion," *IEEE Antennas Wireless Propag. Lett.*, vol. 16, pp. 1048–1051, Oct. 2016.
[25] E. Suter and J. R. Mosig, "A subdomain multilevel approach for the efficient MoM analysis of large planar antennas," *Microw. Opt. Technol. Lett.*, vol. 26, no. 4, pp. 270–277, Aug. 2000.
[26] X.-C. Nie, L.-W. Li, and N. Yuan, "Precorrected-FFT algorithm for solving combined field integral equations in electromagnetic scattering," in *Proc. IEEE AP-S Int. Symp.*, San Antonio, TX, USA, Jun. 2002, pp. 574–577.
[27] S. M. Rao, D. R. Wilton, and A. W. Glisson, "Electromagnetic scattering by surfaces of arbitrary shape," *IEEE Trans. Antennas Propag.*, vol. AP-30, no. 3, pp. 409–418, May 1982.
[28] W. C. Gibson, *The Method of Moments in Electromagnetics*. London, U.K.: Chapman & Hall, 2008.
[29] D. A. Dunavant, "High degree efficient symmetrical Gaussian quadrature rules for the triangle," *Int. J. Numer. Methods Eng.*, vol. 21, no. 6, pp. 1129–1148, 1985.
[30] L. R. Rabiner and R. Gold, *Theory and Application of Digital Signal Processing*. Englewood Cliffs, NJ, USA: Prentice-Hall, 1975.
[31] S. Hubert, S. N. Jha, and C. Craeye, "Layered Green's functions estimation with Contour-FFT," in *Proc. Eur. Conf. Antennas Propag.*, Apr. 2016, pp. 1–4.
[32] S. Hubert, S. N. Jha, and C. Craeye, "Error analysis for the Contour-FFT based Green's function evaluation," in *Proc. Int. Conf. Electromagn. Adv. Appl.*, Sep. 2015, pp. 922–925.
[33] Q. Gueuning, S. Hubert, C. Craeye, and C. Oestges, "Error model for Contour-FFT evaluation of the free-space on-plane Green's function," in *Proc. Int. Symp. Electromagn. Theory*, Aug. 2016, pp. 312–314.
[34] D. Pissoort, E. Michielssen, D. Vande Ginste, and F. Olyslager, "A rank-revealing preconditioner for the fast integral-equation-based characterization of electromagnetic crystal devices," *Microw. Opt. Technol. Lett.*, vol. 48, no. 4, pp. 783–789, Apr. 2006.
[35] N. A. Ozdemir, D. González-Ovejero, and C. Craeye, "On the relationship between multiple-scattering macro basis functions and Krylov subspace iterative methods," *IEEE Trans. Antennas Propag.*, vol. 61, no. 4, pp. 2088–2098, Apr. 2013.
[36] C.-F. Wang, F. Ling, and J.-M. Jin, "A fast full-wave analysis of scattering and radiation from large finite arrays of microstrip antennas," *IEEE Trans. Antennas Propag.*, vol. 46, no. 10, pp. 1467–1474, Oct. 1998.
[37] *MATLAB R2015a*, MathWorks, Inc., Natick, MA, USA, 2015.

Simon Hubert (S'16–M'18) was born in Ottignies, Belgium, in 1989. He received the B.Eng., M.Eng., and Ph.D. degrees in electrical engineering from the Université catholique de Louvain (UCL), Louvain-La-Neuve, Belgium, in 2010, 2012, and 2018, respectively.

From 2012 to 2018, he was a Teaching Assistant with UCL, where he was also teaching antenna theory, embedded systems programming, and physics of semiconductor devices. His current research interests include fast numerical methods for metasurface design and analysis and miniature antenna arrays design for direction finding applications.

Shambhu Nath Jha (S'06–M'14) was born in Janakpur, Nepal, in 1978. He received the bachelor's degree (Hons.) in electrical engineering from the Institute of Engineering, Tribhuvan University, Kirtipur, Nepal, in 2001, the European Master of Research in Information and Communication Technologies degree from the Universitat Politécnica de Catalunya, Barcelona, Spain, in 2008, the master's degree (*cum laude*) in electrical engineering from the Université catholique de Louvain (UCL), Louvain-La-Neuve, Belgium, in 2009, the Ph.D. degree in applied sciences (electrical engineering) from UCL in 2014, and the M.Sc. degree (Hons.) in management from Vrije Universiteit Brussel, Brussels, Belgium, in 2016.

He was an R&D Electrical Engineer with Icoms Detections SA, Ottignies-Louvain-la-Neuve, Belgium, from 2014 to 2016, where he was involved in the area of antenna and microwave circuits for radar system for traffic control in a scientific collaboration with UCL, and was also a Research Assistant for fast analysis of antenna arrays and for several government funded projects on antenna system development with UCL from 2009 to 2014. He is currently a Hardware Engineer with Thales Belgium, Tubize, Belgium. His current research interests include optimized antenna and radio system development for various practical applications, strategic value creation in customer requirements in changing innovative environment, and value co-creation.

Dr. Jha was a recipient of the European Commission's Erasmus Mundus Scholarship from 2007 to 2009 and other 13 national and international academic/research grants and fellowships.

Christophe Craeye (M'98–SM'11) was born in Ronse, Belgium, in 1971. He received the bachelor's degree in philosophy, the master's degree in electrical engineering, and the Ph.D. degree in applied sciences from the Université Catholique de Louvain (UCL), Louvain-la-Neuve, Belgium, in 1994 and 1998, respectively.

From 1994 to 1999, he was a Teaching Assistant with UCL and carried out research on the radar signature of the sea surface perturbed by rain, in collaboration with NASA and ESA. He was with the University of Massachusetts, Amherst, MA, USA, in 1999. From 1999 to 2001, he was a Post-Doctoral Researcher with the Eindhoven University of Technology, Eindhoven, The Netherlands. He was with the Netherlands Institute for Research in Astronomy, Dwingeloo, The Netherlands, in 2001. In 2002, he started an antenna research activity with UCL, where he is currently a Professor. He was with the Astrophysics and Detectors Group, University of Cambridge, Cambridge, U.K., in 2011. His current research interests include mutual coupling, finite antenna arrays, wideband antennas, small antennas, metamaterials, fast physical optics, and numerical methods for the fields in periodic media, with applications to communication and sensing systems.

Dr. Craeye was a recipient of the 2005–2008 Georges Vanderlinden Prize from the Belgian Royal Academy of Sciences in 2009. He was an Associate Editor of the IEEE TRANSACTIONS ON ANTENNAS AND PROPAGATION from 2004 to 2010 and IEEE ANTENNAS AND WIRELESS PROPAGATION LETTERS from 2011 to 2017. His research was funded by the Région Wallonne, European Commission, ESA, Fonds National de la Recherche Scientifique, and UCL.